

Transverse flow in thin superhydrophobic channels

François Feuillebois,¹ Martin Z. Bazant,² and Olga I. Vinogradova^{3,4}

¹LIMSI, UPR 3251, CNRS, B.P. 133, 91403 Orsay, France

²Departments of Mathematics and Chemical Engineering, Massachusetts Institute of Technology, Cambridge, Massachusetts 02139, USA

³A.N. Frumkin Institute of Physical Chemistry and Electrochemistry, Russian Academy of Sciences, 31 Leninsky Prospekt, 119991 Moscow, Russia

⁴ITMC and DWI, RWTH Aachen, Pauwelsstr. 8, 52056 Aachen, Germany

(Received 7 July 2010; revised manuscript received 5 October 2010; published 10 November 2010)

We provide some general theoretical results to guide the optimization of transverse hydrodynamic phenomena in superhydrophobic channels. Our focus is on the canonical micro- and nanofluidic geometry of a parallel-plate channel with an arbitrary two-component (low-slip and high-slip) coarse texture, varying on scales larger than the channel thickness. By analyzing rigorous bounds on the permeability, over all possible patterns, we optimize the area fractions, slip lengths, geometry, and orientation of the surface texture to maximize transverse flow. In the case of two aligned striped surfaces, very strong transverse flows are possible. Optimized superhydrophobic surfaces may find applications in passive microfluidic mixing and amplification of transverse electrokinetic phenomena.

DOI: [10.1103/PhysRevE.82.055301](https://doi.org/10.1103/PhysRevE.82.055301)

PACS number(s): 47.61.-k, 68.08.-p, 83.50.Rp

I. INTRODUCTION

Hydrophobic solid surfaces with special textures can exhibit greatly enhanced (“super”) properties, compared to analogous flat or slightly disordered surfaces [1]. At the microscopic scale, superhydrophobic surfaces could revolutionize microfluidic lab-on-a-chip systems [2], which are becoming widely used in biotechnology. The large effective slip length (the distance within the solid at which the flow profile extrapolates to zero [3–5]) of superhydrophobic surfaces [6,7] compared to simple, smooth channels [8–10] can greatly lower the viscous drag of thin microchannels and reduce the tendency for clogging or adhesion of suspended analytes. Superhydrophobic surfaces can also amplify electrokinetic pumping or energy conversion in microfluidic devices, if diffuse charge in the liquid extends over the gas regions [11,12].

Superhydrophobic surfaces in nature (e.g., the lotus leaf) are typically isotropic, but microfabrication has opened the possibility of highly anisotropic textures [1]. The effective hydrodynamic slip [2,13] (or electro-osmotic mobility [12]) of anisotropic textured surfaces is generally *tensorial*, due to secondary flows *transverse* to the direction of the applied pressure gradient (or electric field [14]). In the case of grooved no-slip surfaces (Wenzel state), transverse viscous flows have been analyzed for small height variations [15] and thick channels [16], and herringbone patterns have been designed to achieve passive chaotic mixing during pressure-driven flow through a microchannel [17–19]. Convection is often required to mix large molecules, reagents, or cells in lab-on-a-chip devices, and passive mixing by textured surfaces can be simpler and more robust than mechanical or electrical actuation. In principle, these effects may be amplified by hydrodynamic slip (in particular in Cassie state when the recessed regions of the texture are filled with gas) and large amplitude roughness (in Wenzel state, when liquid follows the topological variations of the surface), but we are not aware of any prior work.

In this paper, we present some general theoretical results to guide the optimization of transverse hydrodynamic phenomena in a thin superhydrophobic channel. We consider an arbitrary coarse texture, varying on scales larger than the channel thickness, and optimize its orientation and geometry to maximize pressure-driven transverse flow. Our consideration is based on the theory of heterogeneous porous materials [20], which allows us to derive bounds on transverse flow over all possible patterns [7].

II. GENERAL CONSIDERATIONS

We consider the pressure-driven flow of a viscous fluid between two textured parallel plates (“+” and “−”) separated by $h(x, y)$, as sketched in Fig. 1. Channel thickness, h , is assumed to vary slowly in directions x and y along the plates. We assume a very general situation, where sectors of different h are characterized by spatially varying, piecewise constant, slip lengths $b^+(x, y)$ and $b^-(x, y)$.

To evaluate the transverse flow, we calculate the velocity profile and integrate it across the channel to obtain the depth-averaged velocity \mathbf{u} in terms of the pressure gradient ∇p

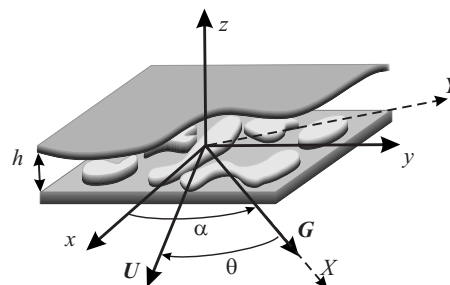


FIG. 1. Sketch of a thin channel of thickness $h(x, y)$ with notation for directions along the plates. In the Wenzel state the liquid would conform the solid surface, but in the Cassie state it remains free-standing at the top of the roughness.

along the plates. As usual for the Hele-Shaw cell, the result may be written as a Darcy law

$$\mathbf{u} = -\frac{k}{\mu} \nabla p, \quad (1)$$

where the local permeability is

$$k = \frac{h^2}{12} \left[1 + \frac{3(\beta^+ + \beta^- + 4\beta^+\beta^-)}{1 + \beta^+ + \beta^-} \right], \quad (2)$$

with $\beta^+ = b^+/h$ and $\beta^- = b^-/h$. Averaging Eq. (1) over the heterogeneities in h, β^+, β^- (see [7] for details), we obtain

$$\mathbf{U} = -\frac{\mathbf{k}^*}{\mu} \cdot \nabla P, \quad (3)$$

where \mathbf{U}, P denote the averages of \mathbf{u}, p , respectively. To simplify the notation, let $\mathbf{G} = -(1/\mu) \nabla P$ and $G = |\mathbf{G}|$.

A general inhomogeneous medium is characterized by an effective permeability tensor \mathbf{k}^* with eigenvalues k_{\parallel} along x and k_{\perp} along y , where $k_{\parallel} \geq k_{\perp} > 0$. The vector \mathbf{G} is applied at an angle α to x . Due to inhomogeneity, the velocity \mathbf{U} is generally at an angle θ ($0 \leq |\theta| \leq \pi/2$) with respect to \mathbf{G} . Since $k_{\parallel} \geq k_{\perp}$, it is expected that \mathbf{U} will be preferentially in the direction of x . Letting X be the direction of \mathbf{G} , and Y the perpendicular direction along the plates, we obtain

$$U_x = k_{\parallel} G \cos \alpha \quad U_y = k_{\perp} G \sin \alpha,$$

$$U_X = U_x \cos \alpha + U_y \sin \alpha = G(k_{\parallel} \cos^2 \alpha + k_{\perp} \sin^2 \alpha),$$

$$U_Y = -U_x \sin \alpha + U_y \cos \alpha = G(-k_{\parallel} + k_{\perp}) \sin \alpha \cos \alpha.$$

Our aim is to optimize the texture and the angle α , so that the angle θ between \mathbf{U} and \mathbf{G} is maximum providing the best transverse flow. That is, $|U_Y/U_X|$ should be maximum (note that $U_Y < 0$ here). Since at $\alpha=0$ and $\pi/2$, $U_Y=0$, these cases are readily eliminated (The case of small but nonzero $|\pi/2 - \alpha|$ may be included in the general framework, as will be discussed below). It is easy to show that

$$\left| \frac{U_Y}{U_X} \right| = \frac{(k_{\parallel} - k_{\perp}) \sin \alpha \cos \alpha}{k_{\parallel} \cos^2 \alpha + k_{\perp} \sin^2 \alpha} = \frac{(\lambda^2 - 1)t}{\lambda^2 + t^2}, \quad (4)$$

with $\lambda^2 = k_{\parallel}/k_{\perp} \geq 1$ and $t = \tan \alpha$, is at a maximum if $t = \lambda$. The value of the maximum is

$$\left| \frac{U_Y}{U_X} \right| = \frac{1}{2} \left(\lambda - \frac{1}{\lambda} \right)$$

and then $\theta = \pi/2 - 2\alpha$ (the direction of \mathbf{U} is $\pi/2 - \alpha$). Therefore, we have transformed our task to optimization of λ . To maximize U_Y/U_X , λ should be as large as possible (Fig. 2), i.e., k_{\parallel} should be as large, and k_{\perp} should be as small as possible.

III. TWO-COMPONENT MEDIUM

In order to proceed further, the analysis is now restricted to a two-component anisotropic medium with permeabilities k_1, k_2 . Consider without loss of generality that $0 \leq k_1 < k_2$

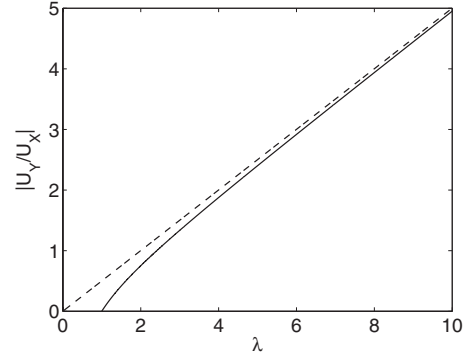


FIG. 2. The ratio of velocity components, $|U_Y/U_X|$, as a function of $\lambda = \sqrt{k_{\parallel}/k_{\perp}}$.

$< \infty$. The largest possible k_{\parallel} corresponds to the upper Wiener bound [20],

$$k_{\parallel} = \phi_1 k_1 + \phi_2 k_2,$$

where ϕ_1 and ϕ_2 are the area fractions of the two phases with $\phi_1 + \phi_2 = 1$. The smallest possible k_{\perp} corresponds to the lower Wiener bound,

$$k_{\perp} = \left(\frac{\phi_1}{k_1} + \frac{\phi_2}{k_2} \right)^{-1}.$$

A texture satisfying simultaneously both conditions exists: it is a configuration of stripes.

We then have for this texture

$$\lambda^2 = \frac{k_{\parallel}}{k_{\perp}} = 1 + \phi_1(1 - \phi_1) \frac{(k_1 - k_2)^2}{k_1 k_2}.$$

The surface fraction ϕ_1 corresponding to a maximum of U_Y/U_X can be found from the equation

$$\frac{\partial}{\partial \phi_1} \left| \frac{U_Y}{U_X} \right| = \frac{1}{2} \left(1 + \frac{1}{\lambda^2} \right) \frac{1}{2\lambda} \frac{\partial \lambda^2}{\partial \phi_1} = 0,$$

which leads to $\partial \lambda^2 / \partial \phi_1 = 0$, which is satisfied at $\phi_1 = 1/2$. This extremum corresponds to a maximum and then

$$\lambda^2 = 1 + \frac{(k_1 - k_2)^2}{4k_1 k_2} = \frac{(k_1 + k_2)^2}{4k_1 k_2}.$$

Defining

$$\bar{k} = \frac{k_1 + k_2}{2}, \quad \langle k \rangle = \sqrt{k_1 k_2},$$

the maximum occurs at

$$\lambda = \frac{\bar{k}}{\langle k \rangle} \quad (5)$$

and its value is

$$\left| \frac{U_Y}{U_X} \right| = \frac{1}{2} \left(\frac{\bar{k}}{\langle k \rangle} - \frac{\langle k \rangle}{\bar{k}} \right) = \frac{1}{2} \left[\frac{1 + k_2/k_1}{2\sqrt{k_2/k_1}} - \frac{2\sqrt{k_2/k_1}}{1 + k_2/k_1} \right], \quad (6)$$

which increases monotonously with the anisotropy, k_2/k_1 . It is interesting to note that the preceding analysis applies to any incompressible, gradient-driven “flow” in a two-component medium, not only fluid flow, but also electrical conduction (in which case, we have maximized the transverse current).

IV. SUPERHYDROPHOBIC CHANNELS

We now apply these results to transverse viscous flow in textured, slipping microchannels. We focus first on rough hydrophobic surfaces in the Cassie state, where trapped air bubbles [21] can lead to dramatic local slip enhancement. To model this, we assume the liquid surface is approximately flat, so the local channel thickness $h=H$ is fixed. This common assumption also corresponds to the minimum dissipation [6]. The liquid contacts the solid only over an area fraction ϕ_1 of the surface with slip length b_1 , while the remaining area fraction ϕ_2 is a free-standing gas-liquid interface. As a simple estimate, lubricating gas sectors of height δ with viscosity μ_g much smaller than that of the liquid μ [22] have a local slip length $b_2 \approx \delta(\mu/\mu_g) \approx 50\delta$, which can reach tens of μm . Hydrodynamic slip can also occur at solid hydrophobic sectors [3–5], but with b_1 less than tens of nm [8–10].

We now consider two cases [7]: (I) one slip wall ($\beta^+ = \beta$; $\beta^- = 0$), and (II) equal slip on opposite surfaces ($\beta^+ = \beta^- = \beta$). Case (I) is relevant for various setups where the alignment of opposite textures is inconvenient or difficult. Case (II) is normally used to minimize the drag [7]. In each case, we have a two-component medium where β is either β_1 or β_2 . The permeability can now be expressed in term of the gap and slip lengths, Eq. (2). Then, for $j=1, 2$,

$$k_j = \frac{h^2}{12} \begin{cases} 1 + 3\beta_j/[1 + \beta_j] & \text{case (I)} \\ 1 + 6\beta_j & \text{case (II)} \end{cases}. \quad (7)$$

Since h is constant, the largest k_2/k_1 obviously corresponds to a largest physically possible β_2 with smallest possible β_1 , that is $\beta_1=0$.

In case (I), approximating the largest possible β_2 by $\beta_2 \rightarrow \infty$ gives $k_2/k_1=4$. We obtain $\lambda = \bar{k}/\langle k \rangle = 5/4$. The direction of \mathbf{G} is $\alpha = \arctan(5/4) = 51.34^\circ$. Then $|U_Y/U_X| \rightarrow 9/40 = 0.225$. The direction of \mathbf{U} is $90^\circ - \alpha = 38.66^\circ$ [see Fig. 3(a)], corresponding to a maximum deflection of almost 13° .

In case (II), the deflection can be more dramatic, but the analysis is more subtle. For $\beta_2 \gg 1$, $k_2 \approx 6\beta_2$, the angle α is close to $\pi/2$. Depending on which of the two limits $\beta_2 \rightarrow \infty$ and $\alpha \rightarrow \pi/2$ is taken first, the results are different. This is a singular perturbation problem. Our optimum gives here the *significant degeneracy* [23], that is the most general limit from which any case may be obtained [24]. We then calculate the following first order approximation:

$$\alpha \approx \frac{\pi}{2} - \sqrt{\frac{2(1 + 6\beta_1)}{3\beta_2}},$$

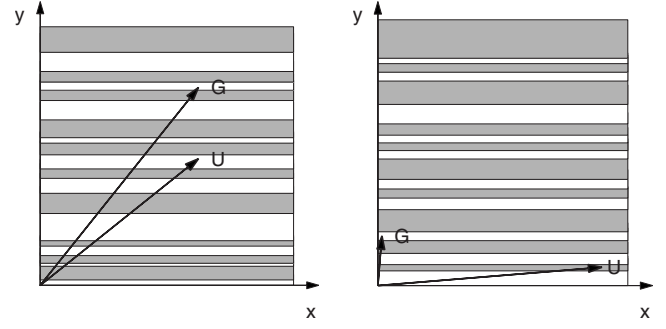


FIG. 3. Cassie state. Results of transverse flow optimization for flat microchannels in case I (left) and case II (right). In both cases, the thickness of stripes is taken as random, to emphasize that the design does not have to be periodic. The mean surface fraction of each component is 1/2. As an example, the distribution of thicknesses is Gaussian with a standard deviation of 0.2. For case II, $\beta_2=100$, and $U_x \approx 300G$ has been shortened for visibility.

$$U_X \approx 4G(1 + 6\beta_1), \quad U_Y \approx -\sqrt{6\beta_2(1 + 6\beta_1)}G.$$

The angle of \mathbf{U} and \mathbf{G} is then $\theta \approx \pi/2 - 2\sqrt{2(1 + 6\beta_1)}/3\beta_2$. Note that the flow in this direction close to $\alpha = \pi/2$ is large, but is yet $O(\sqrt{\beta_2})$ smaller than the flow that would exist in the X direction for $\alpha=0$.

For completeness, we also apply our results to the Wenzel state, where the liquid is assumed to follow all the topological variations of the material. This leads to a variable thickness for the liquid domain, but fixed hydrodynamic boundary condition. Therefore, the slip length b is uniform (possibly zero), but channel thickness h may take two values, H_1 and H_2 ($H_2 > H_1$). For both cases I and II, it is easy then to show [24] that k_2/k_1 increases with H_2/H_1 for fixed $\beta = b/H_1$. The variation of k_2/k_1 with H_2/H_1 and β in cases I and II is shown as contour plots in Fig. 4. Replacing this value of k_2/k_1 in Eq. (6) shows that H_2/H_1 should be as large as possible. This limit is very different from the small surface height modulations and lubrication geometries considered by Stroock *et al.* [17] and suggests that further improvements in passive chaotic mixers may be possible with deeper grooves and thinner channels.

V. CONCLUDING REMARKS

A striking conclusion from our analysis is that the surface textures which optimize transverse flow can significantly dif-

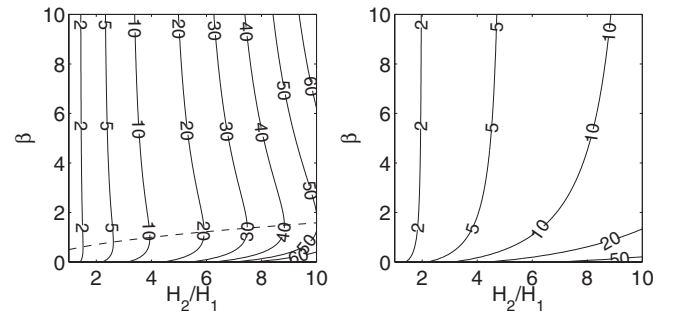


FIG. 4. Wenzel state. Contour plot of k_2/k_1 with H_2/H_1 and β in cases I (left) and II (right). The dashed line (left) represents the minimum of k_2/k_1 with β for constant H_2/H_1 .

fer from those optimizing effective (forward) slip. It is well known that the effective slip of a superhydrophobic surface is maximized by reducing the solid-liquid area fraction ϕ_1 [6,7], until the Cassie state becomes metastable [1]. In contrast, we have shown that transverse flow in thin channels is maximized by stripes with a rather large solid fraction, $\phi_1 = 1/2$, where the Cassie state is typically stable. In this situation, the effective slip β^* is relatively small [7], and yet the flow deflection is very strong (nearly $\pi/2$).

These results may guide the design of superhydrophobic surfaces for robust transverse flows in microfluidic devices. Applications may include flow detection, droplet or particle sorting, or passive mixing. The latter results from interactions with side walls in a direction X at an angle $\pi/2 - \alpha$ with x . The pressure gradient component G_X along the walls creates an average Poiseuille flow U_X . In the normal direction, G_Y induces a quadratic recirculation flow velocity with zero average $U_Y = 0$. With one slip plane (case I) this flow has one vortex and with two slip planes (case II) two counter-rotating vortices. The recirculation is optimum for maximum $|G_Y/G_X| = (\lambda^2 - 1)t/(\lambda^2 + t^2)$. By comparison with Eq. (4), the above optimization procedure applies and results are identical. Combining flows along X and Y produces helical streamlines. These streamlines can be made chaotic for efficient mixing by modulating the surface texture in the axial direc-

tion, e.g., with herringbone patterns [15,17–19]. Compared to the grooved no-slip surfaces with small height variations used in prior work, we have shown that slipping (Cassie) and highly rough (Wenzel) surfaces can exhibit much stronger flow deflection in thin channels, which could lead to more efficient mixing upon spatial modulation of the texture.

Another fruitful direction could be to consider transverse electrokinetic phenomena [14], e.g., for flow sensors or electro-osmotic pumps [25]. It was recently shown that flat superhydrophobic surfaces can exhibit tensorial electro-osmotic mobility [12]: Anisotropy is maximized if the Debye screening length λ_D is comparable to the texture scale, and the gas-liquid interface is uncharged (which, again, does not maximize forward flow); the electro-osmotic mobility scales as, $\mathbf{M}_e \propto (\mathbf{I} + \mathbf{b}/\lambda_D)$ in the limit of thick double layers and even thicker channels ($L \ll \lambda_D \ll H$) [12]. If a similar relation holds for thin channels ($H \ll L \ll \lambda_D$), then our results for the effective \mathbf{b} (from \mathbf{k} in case II [7]) suggest that transverse electrokinetic phenomena could be greatly amplified by using striped superhydrophobic surfaces.

This research was partly supported by the DFG under the Priority program “Micro and nanofluidics” (Grant No. Vi 243/1-3).

-
- [1] D. Quere, *Annu. Rev. Mater. Res.* **38**, 71 (2008).
 [2] H. A. Stone, A. D. Stroock, and A. Ajdari, *Annu. Rev. Fluid Mech.* **36**, 381 (2004).
 [3] O. I. Vinogradova, *Int. J. Min. Process.* **56**, 31 (1999).
 [4] E. Lauga, M. P. Brenner, and H. A. Stone, *Handbook of Experimental Fluid Dynamics* (Springer, New York, 2007), Chap. 19, pp. 1219–1240.
 [5] L. Bocquet and J. L. Barrat, *Soft Matter* **3**, 685 (2007).
 [6] C. Ybert, C. Barentin, C. Cottin-Bizonne, P. Joseph, and L. Bocquet, *Phys. Fluids* **19**, 123601 (2007).
 [7] F. Feuillebois, M. Z. Bazant, and O. I. Vinogradova, *Phys. Rev. Lett.* **102**, 026001 (2009).
 [8] O. I. Vinogradova, K. Koynov, A. Best, and F. Feuillebois, *Phys. Rev. Lett.* **102**, 118302 (2009).
 [9] O. I. Vinogradova and G. E. Yakubov, *Langmuir* **19**, 1227 (2003).
 [10] C. Cottin-Bizonne, B. Cross, A. Steinberger, and E. Charlaix, *Phys. Rev. Lett.* **94**, 056102 (2005).
 [11] T. M. Squires, *Phys. Fluids* **20**, 092105 (2008).
 [12] S. S. Bahga, O. I. Vinogradova, and M. Z. Bazant, *J. Fluid Mech.* **644**, 245 (2010).
 [13] M. Z. Bazant and O. I. Vinogradova, *J. Fluid Mech.* **613**, 125 (2008).
 [14] A. Ajdari, *Phys. Rev. E* **65**, 016301 (2001).
 [15] A. D. Stroock, S. K. W. Dertinger, A. Ajdari, I. Mezić, H. A. Stone, and G. M. Whitesides, *Science* **295**, 647 (2002).
 [16] C. Y. Wang, *Phys. Fluids* **15**, 1114 (2003).
 [17] A. D. Stroock, S. K. Dertinger, G. M. Whitesides, and A. Ajdari, *Anal. Chem.* **74**, 5306 (2002).
 [18] A. D. Stroock and G. J. McGraw, *Philos. Trans. R. Soc. London, Ser. A* **362**, 971 (2004).
 [19] E. Villiermaux, A. D. Stroock, and H. A. Stone, *Phys. Rev. E* **77**, 015301 (2008).
 [20] S. Torquato, *Random Heterogeneous Materials: Microstructure and Macroscopic Properties* (Springer, New York, 2002).
 [21] C. Cottin-Bizonne, C. Barentin, E. Charlaix, L. Bocquet, and J. L. Barrat, *Eur. Phys. J. E* **15**, 427 (2004).
 [22] O. I. Vinogradova, *Langmuir* **11**, 2213 (1995).
 [23] W. Eckhaus, *Asymptotic Analysis of Singular Perturbations*, Studies in Applied Mathematics Vol. 9 (North-Holland, Amsterdam, 1979).
 [24] See supplementary material at <http://link.aps.org/supplemental/10.1103/PhysRevE.82.055301> for details of analysis.
 [25] I. Gitlin, A. D. Stroock, G. M. Whitesides, and A. Ajdari, *Appl. Phys. Lett.* **83**, 1486 (2003).